Since January 2020 Elsevier has created a COVID-19 resource centre with free information in English and Mandarin on the novel coronavirus COVID-19. The COVID-19 resource centre is hosted on Elsevier Connect, the company's public news and information website.

Computers in Biology and Medicine 135 (2021) 104525

Contents lists available at ScienceDirect

Computers in Biology and Medicine

journal homepage: www.elsevier.com/locate/compbiomed

Unravelling the therapeutic potential of marine drugs as SARS-CoV-2 inhibitors: An insight from essential dynamics and free energy landscape

Shailima Rampogu [a,c,*], Rajesh Goud Gajula [b], Gihwan Lee [a], Myeong Ok Kim [c,**], Keun Woo Lee [a,***]

[a] Division of Life Sciences, Division of Applied Life Science (BK21 Plus), Research Institute of Natural Science (RINS), Gyeongsang National University (GNU), 501 Jinju-daero, Jinju, 52828, South Korea

[b] Primer Biotech Research Center, Jaipuri Colony, Nagole, Hyderabad, Telangana, 500068, India

[c] Division of Life Science and Applied Life Science (BK 21 Plus), College of Natural Sciences, Gyeongsang National University, Jinju, South Korea

ARTICLE INFO

Keywords:
COVID-19
Marine drugs/ derivatives
Essential dynamics
Free energy landscape
And main protease

ABSTRACT

Coronavirus disease 2019 (COVID-19) is an ongoing pandemic. The virus that causes the disease, severe acute respiratory syndrome coronavirus-2 (SARS-CoV-2), predominantly infects the respiratory tract, which may lead to pneumonia and death in severe cases. Many marine compounds have been found to have immense medicinal value and have gained approval from the Food and Drug Administration (FDA), and some are being tested in clinical trials. In the current investigation, we redirected a number of marine compounds toward SARS-CoV-2 by targeting the main protease (M^{pro}, PDB ID: 6Y2F), subjecting them to several advanced computational techniques using co-crystallised ligand as the reference compound. The results of the binding affinity studies showed that two compounds, eribulin mesylate (eri) and soblidotin (sob), displayed higher docking scores than did the reference compound. When these compounds were assessed using molecular dynamics simulation, it was evident that they demonstrated stable binding at the binding pocket of the target protein. The systems demonstrated stable root mean square deviation and radius of gyration values, while occupying the binding pocket during the simulation run. Furthermore, the essential dynamics and free energy landscape exploration revealed that the protein had navigated through a minimal energy basin and demonstrated favourable conformation while binding to the proposed inhibitors. Collectively, our findings suggest that two marine compounds, namely eri and sob, show potential as SARS-CoV-2 main protease inhibitors.

1. Introduction

Coronavirus disease 2019 (COVID-19) is caused by severe acute respiratory syndrome coronavirus-2 (SARS-CoV-2) [1]. Infection, which is often manifested as fever and cough, may lead to pneumonia [2,3]. Coronaviruses (CoVs) belong to the Coronaviridae family and possess a large single-stranded RNA genome [4]. Of the four identified classes of Coronaviridae, SARS-CoV-2 is classified into the beta genera, which includes Severe Acute Respiratory Syndrome (SARS) and Middle East Respiratory Syndrome (MERS) [5]. Upon analysing the genome of COVID-19, two large polyproteins were detected, ORF1a and ORF1b (ORF1ab), along with four structural and six accessory proteins. The polyprotein is cleaved to generate 16 non-structural proteins (nsps) [6–8]. The structural proteins are the envelope protein (E), membrane protein (M), nucleocapsid (N), and spike protein (S). The spike protein of the virus facilitates the entry of the virus into the host (human) when attached to the receptor protein, angiotensin-converting enzyme 2 (ACE2). This is followed by the generation of nsps that promote the replication of the virus [9,10].

Although a host of drugs has been used against the disease and some of them have reached clinical trials [11], the search for an effective drug is still under investigation. In a number of recent studies, drug repurposing approaches have been applied, employing both computational and experimental methods [12–21]. However, the need for effective

* Corresponding author. Division of Life Sciences, Division of Applied Life Science (BK21 Plus), Research Institute of Natural Science (RINS), Gyeongsang National University (GNU), 501 Jinju-daero, Jinju, 52828, South Korea.
** Corresponding author.
*** Corresponding author.
E-mail addresses: shailima.rampogu@gmail.com (S. Rampogu), mokim@gnu.ac.kr (M.O. Kim), kwlee@gnu.ac.kr (K.W. Lee).

https://doi.org/10.1016/j.compbiomed.2021.104525
Received 4 March 2021; Received in revised form 20 May 2021; Accepted 20 May 2021
Available online 29 May 2021

drugs remains. Targeting the proteins involved in viral replication is a superior approach to hindering viral growth and, consequently, its spread [22]. In this study, we aimed to find effective drug candidates against SARS-CoV-2 main protease (M^{pro}), given the evidence that inhibiting M^{pro} leads to the obstruction of viral replication [23].

The viral target M^{pro} has garnered wide attention because of its crucial role in processing the polyproteins as a result of translation from viral RNA [23]. This enzyme performs its functions at no less than 11 cleavage sites located on the larger polyprotein 1 ab. The principal recognising site is Leu-Gln↓(Ser, Ala, and Gly). Interestingly, human proteases with similar cleavage specificity have not been reported, suggesting that the identified inhibitors are nontoxic [23]. Structurally, M^{pro} is made up of three domains: domain I comprises the residues from 8 - 101; domain II consists of the residues from 102 - 184, displaying an antiparallel β-barrel structure; and domain III corresponds to residues 201–303, enclosing five α-helices organised into a large antiparallel globular cluster [24]. Domain III is connected to domain II by a long loop region (residues 185–200). The target protein has a catalytic dyad with Cys-His residues. The substrate-binding site is stationed in a groove located between domains I and II [24]. This site has been explored for the design and discovery of new potential drugs.

Nature offers a variety of sources for drug discovery and development, including plants, animals, microorganisms, and marine organisms [25]. Marine-derived scaffolds are instrumental in adding more compounds to the process of drug discovery and development [25,26].

By 1974, two marine-derived natural products (cytarabine, Ara-C and vidarabine, Ara-A) had been included in pharmacopoeia to treat human disease [27] and a few have gained approval from the U.S. Food and Drug Administration (FDA), while some are in clinical trials [28]. Marine compounds obtained from various sources have been used to treat certain viral diseases [29]. Prior to this, reports exist regarding the use of marine drugs against SARS [30,31]. Interest in marine compounds has increased recently, and the search for novel marine scaffolds for SARS-CoV-2 is now underway. Accordingly, some researchers have focused on the use of computational methods to retrieve potential hits against SARS-CoV-2 [32–35]. Encouraged by these reports, we have repurposed the marine-derived compounds which are FDA approved and are at different phases of clinical trials against M^{pro}, in order to discover putative inhibitors to mitigate the disease.

2. Materials and methods

2.1. Selection and preparation of the target protein

The target chosen for the current investigation was the main protease (M^{pro}) bearing the PDB ID: 6Y2F [23], complexed with the inhibitor O6K [23]. The protein was downloaded in PDB format and upgraded using Discovery Studio v.18 (DS). Subsequently, the presence of gaps and missing residues was assessed using the *Clean Protein* tool accessible on DS and minimised using the *Minimize and Refine Protein* protocol. Prior to refinement, the heteroatoms and water molecules were dislodged [36].

2.2. Selection of the small molecules

The small molecules chosen for the current study were compounds obtained from the marine sources chosen from the literature [28]. Specifically, the research work included the collection of compounds which are approved by the FDA and/or are in the investigative stage, as detailed in Table 1. The small molecules were downloaded from the PubChem database in 2D format and were escalated to the DS to obtain their 3D structures. The ligands were prepared using the *Prepare Ligands* protocol available in DS, which assists in the preparation of ligands by performing tasks such as removing duplicates, enumerating isomers and tautomers, and generating 3D conformations. The prepared ligands were minimised using a *Full Minimization* module available with the DS.

Table 1
List of the marine drugs and derivatives.

Compound name	Marine organism	FDA status
Cytarabine, ara-C	Sponge	Approved
Brentuxlmab vedotin (SGN - 35)	Mollusc/cyanobacterium	
Vidarabine, ara-A	Sponge	
Omega-3-acid ethyl esters	Fish	
Ziconotide	Cone snail	
Eribulin mesylate (E7389)	Sponge	
Trabectedin (ET- 743)	Tunicate	
Plitidepsin	Tunicate	Phase III
Tetrodotoxin	Pufferfish	
Soblidotin (TZT 1027)	Bacterium	
DMXBA (GTS- 2 1)	Worm	Phase II
Plinabulin (NPl-2358)	Fungus	
Elisidepsin	Mollusc	
PM001004	Nudibranch	
Tasidotin, Synthadotin (ILX - 651)	Bacterium	
Pseudopterosins	Soft coral	
Bryostatin 1	Bryozoa	Phase I
Hemiasterlin (E7974)	Sponge	
Marizomib (salinosporamide A)	Bacterium	Preclinical
Chrysophaentin A	Alga *Halobacillus salinu*	
Phenethylamine	Bacterium, lyngbyoic acid	
Geodisterol sulfites	Sponge	
Pseudoalteromonas sp. metabolites	Bacteria	
Peziza vesiculosa β-carboline	Bryozoa	
Bromophycolides	Alga	
Plakortin	Sponge	
Homogentisicacid	Sponge	
Hymenidin	Sponge	
Gyrosanols	Soft coral	
Dysidine	Sponge	
Arenamides A and B	Bacteria	
Capnellene	Soft coral	
Floridosides	Alga	
Grassystatins A- C	Bacteria	
Callyspongidiol	Sponge	
Calyculin A	Sponge	
Pulicatin A	Bacteria	
Dysideamine	Sponge	

2.3. Binding affinity studies and binding energy estimation

Binding affinity studies were performed using the CDOCKER module obtained from DS [37,38]. CDOCKER employs the CHARMm-based molecular dynamics simulation (MDS) method to dock ligands into the receptor-binding site. Correspondingly, random conformations of the ligand were generated using high-temperature MD. These conformations were further translated into binding sites. Subsequently, candidate poses were generated using random rigid-body rotations followed by simulated annealing. A final minimisation was then applied to refine the ligand poses. This programme allows the refinement docking of any number of ligands with a single protein receptor.

The active site was chosen around the inbound ligand for all atoms and residues within a radius of 11 Å. The best pose was chosen based on the highest docking score from the largest cluster, displaying interactions with the key residues. For superior evaluation of the putative inhibitors, the co-crystallised ligand was considered as a reference compound.

The binding free energies were then determined for each ligand and receptor. The free energy of binding for a receptor-ligand complex can be calculated from the free energies of the complex, receptor, and ligand. Here, the binding energies were calculated using the *Calculate Binding Energies* protocol available in DS.

2.4. Stability analysis inferred using MDS

To elucidate the nature of small molecules at the binding pocket of

the protein, MDS was performed with GROMACS v2016.16 [39]. The main objective of using MDS is to estimate the stability of the protein-ligand complex and to delineate the interaction at the atomistic level, as reported earlier [40,41]. The ligand topologies were obtained from SwissParam [42] using the CHARMM27 all-atom force field. A dodecahedron water box consisting of a TIP3P water model was used to solvate the system, and, subsequently, counter ions were added. The system was then minimised, followed by coupling of the protein and ligand. The coupling process was proceeded by a double equilibration method using the conserved number of particles (N), system volume (V), temperature (T) (NVT), and a constant number of particles (N), system pressure (P), and temperature (T) (NPT) for 1 ns each. The NPT ensembles were escalated to the MDS for 100 ns. The pressure of the system was monitored using a Parrinello–Rahman barostat [43]. The protein backbone was restrained, while the solvent molecules and counter ions were permitted to move. The geometry of the molecules was maintained by the LINCS algorithm, which constrained the bond length [44]. All analyses were carried out using visual molecular dynamics (VMD) [45] and DS. The results were evaluated according to the root mean square deviation (RMSD), root mean square fluctuations (RMSF), radius of gyration (Rg) [46], potential energy, number of hydrogen bonds, distance between the hydrogen bond interacting residues and ligand atoms, interaction energy, and the mode of ligand binding. Additionally, the essential dynamics and free energy landscape investigations were carried out to gain a deeper understanding of the dynamics between the protein and ligands [47].

3. Results

3.1. Binding affinity studies and binding energies

Molecular docking between the protein and the ligands was performed to determine the binding affinities between them and predict the predictive binding modes [36]. The selected ligands were allowed to generate 50 conformations and were subsequently clustered. From the largest cluster, the poses with better -CDOCKER interaction energy were chosen as the best poses and lower binding energies, as tabulated in Table 2. Two compounds, eribulin (eri) mesylate [48] and soblidotin (sob) showed a better binding score than the reference compound complemented by the largest cluster. Additionally, these compounds have demonstrated interactions with key residues in the binding pocket of the protein. Correspondingly, the best complexes obtained were upgraded to MDS studies to gain deeper insights.

Table 2
Binding affinity results and intermolecular interactions.

Compound name	Docking score[a]	Hydrogen bonds	π/Alkyl/ sulfur interactions	Van der Waals	Binding energy[b]
Eribulin mesylate (eri)	68.48	Glu166: O–H109 Met165: SD-H110	Pro168	Thr25, Leu27, His41, Asn142, Gly143, Cys145, His164, Leu167, and Thr190	−96.60
Soblidotin (sob)	68.00	Cys44: O–H84 Asn142: HD21-O6 Asn142: HD22-O6	Met165	Thr25, Thr26, Leu27, His41, Val42, Cys44, Thr45, Glu47, Asp48, Met49, Tyr54, Cys145, Leu167, Pro168, His164, Arg188, Asp187, and Gln189	−76.32
Reference (ref)	58.50	His41: NE2-H65 Ser144: HN–O28 Cys145: HN–O28 Glu166: O–H53 Glu166: HN–O11	His164, Pro168	Thr25, Thr26, Leu27, Gly143, Leu167, Val186, Asp187, and Gln189	−65.04

[a] Interaction energy (¯CDOCKER) is expressed in kcal/mol.
[b] Binding energy is expressed in kcal/mol.

3.2. Stability analysis inferred using MDS

To elucidate the behaviour of small molecules at the binding pocket of the target, an MDS study was conducted. MDS serves as an alternative to experimental limitations and can simulate the system at the atomistic scale [49]. The obtained results were assessed according to the RMSD, radius of gyration (Rg), potential energy, RMSF, mode of ligand binding, number of hydrogen bond analysis, distance measure, and interaction energy.

3.3. RMSD

The protein stability corresponding to its conformation can be judged by the variations generated, if any, while the simulation period rationally inferred that smaller deviations greater the stability of the protein [50]. The RMSD profiles were plotted for the backbone atoms of the protein to determine if there were any significant deviations in the graphs. The three systems have projected the RMSD plots below 0.3 nm, with an average of 0.17, 0.17, and 0.18 nm, respectively, for the reference compound (ref), eri, and sob. Additionally, we measured the RMSD of the complexes to explore the stability dynamics of the protein with its respective ligand complexes. The obtained results show that the protein-ref, protein-eri, and protein-sob complexes displayed an RMSD of 0.23, 0.23, and 0.24 nm, respectively. Although the complexes showed a slight increase in the RMSD profiles, they were still within the acceptable range. These findings indicate that the systems are stable, as shown in Fig. 1a.

3.4. Radius of gyration

Protein structure compactness is measured as the radius of gyration (Rg), inferring that the three-state folding of proteins is more compact than that of proteins in two-state folding [51]. In the present study, the compactness of the protein backbone was studied during the entire simulation run. It was noted that the protein was highly stable, with an Rg value ranging from 2.16 to 2.28 nm, as shown in Fig. 1b. While ref and eri demonstrated firm Rg values, sob showed a peak at 93,920 ps, which decreased to a plateau at 94,910 ps, and a steady equilibrium was noted thereafter, as shown in Fig. 1b and Supplementary Figure 1. Overall, the three systems were firmly compact.

3.5. Potential energy

Another parameter, the potential energy, was also calculated. The three systems established a steady potential energy, between −834,000 and −827,000 kJ/mol, as shown in Fig. 1c. The average potential energy was calculated as −830653 kJ/mol for ref, −830,859 kJ/mol for eri, and −831,126 kJ/mol for sob. These results reinforce the reasoning that the systems were stable, with no major fluctuations.

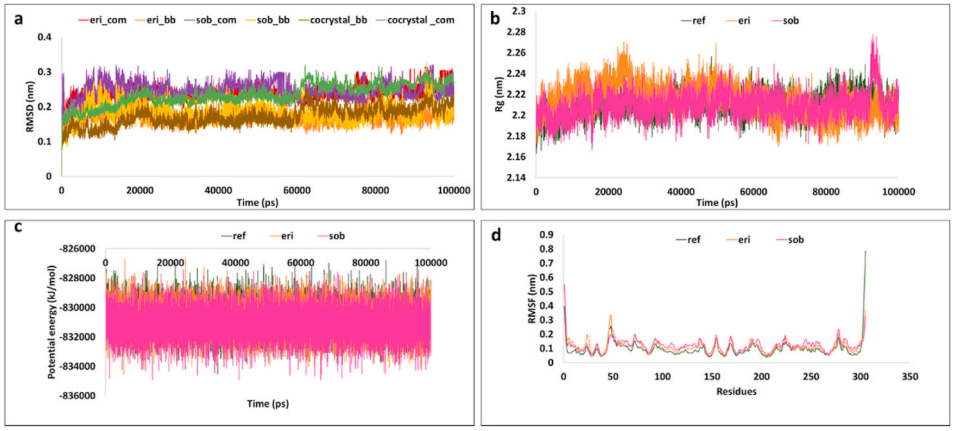

Fig. 1. Stability analysis using molecular dynamics simulation. (a) Root mean square deviation (RMSD) of the backbone. (b) Compactness assessment guided by the radius of gyration (Rg). (c) Examination of the potential energy profiles. (d) Assessing stability based on RMSF of fluctuations of the protein. bb, backbone; com, complex; ref, reference compound; eri, eribulin; sob, soblidotin.

3.6. RMSF

RMSF is defined as a measure of residue-specific flexibility [52]. Here, RMSF was conducted on the protein backbone of the three systems. No fluctuations were observed in the backbone residues, as shown in Fig. 1d. It is noteworthy that Asp48 appeared to have shown marginal fluctuations from the loop region. Interestingly, this residue was not a major part of the binding pocket. Barring Asp48, the remaining residues were highly stable (without any fluctuations), maintaining the integrity of the target protein.

3.7. Binding mode analysis

From the stable RMSD, the last 5 ns structure was extracted and subsequently superimposed against the X-ray crystal structure. The results showed that the compounds were accommodated at the binding pocket as that of the innate compound O6K, as shown in Fig. 2, surrounded by key residues.

3.8. Hydrogen bond interactions and distance between the interacting residues and atoms

The hydrogen bond interactions were monitored throughout the simulations. The obtained results indicate that the hydrogen bonds were persistent throughout the simulation run for all three systems. Furthermore, the hydrogen bonds ranged between 1 and 9, with an average of 2.5, 1.9, and 2.1, respectively, for ref, eri, and sob, as shown in Fig. 3a. These results suggest that the ligand interacts with the target protein during the entire simulation and lies within the binding pocket.

The intermolecular interactions showed that the ref compound formed four hydrogen bonds with the residues His41, Ser144, Cys145, and Glu166, respectively, as shown in Fig. 4a and Table 2, rendered by an acceptable bond length. This compound formed interactions via alkyl and π-alkyl interactions with the residues His164 and Pro168. Notably, the residue Met49 formed a π-sulfur linkage and Met165 formed carbon hydrogen bonds. Furthermore, the residues Thr25, Thr26, Leu27, Gly143, Leu167, Val186, Asp187, and Gln189 held the ligand via van

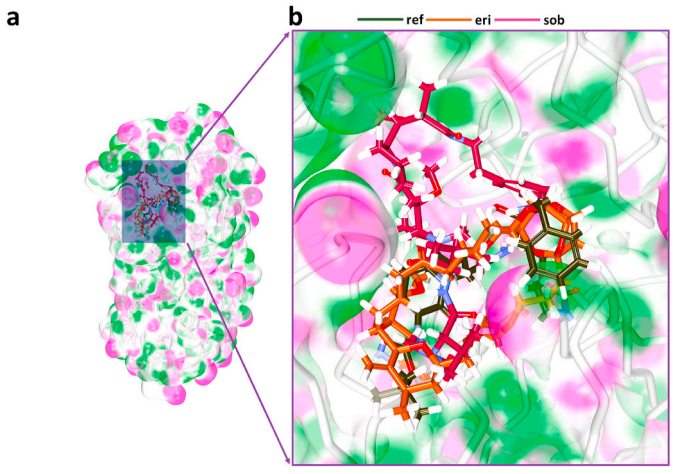

Fig. 2. Accommodation of the compounds at the binding pocket of the protein. (a) Binding mode of the discovered marine compounds in comparison with the reference compound. (b) Magnified version of image in (a). The surface of the protein is represented in colour according to hydrogen bond donor/acceptor model. The protein, PDB ID: 6Y2F, is represented in tube format, and the small molecules are illustrated in stick format.

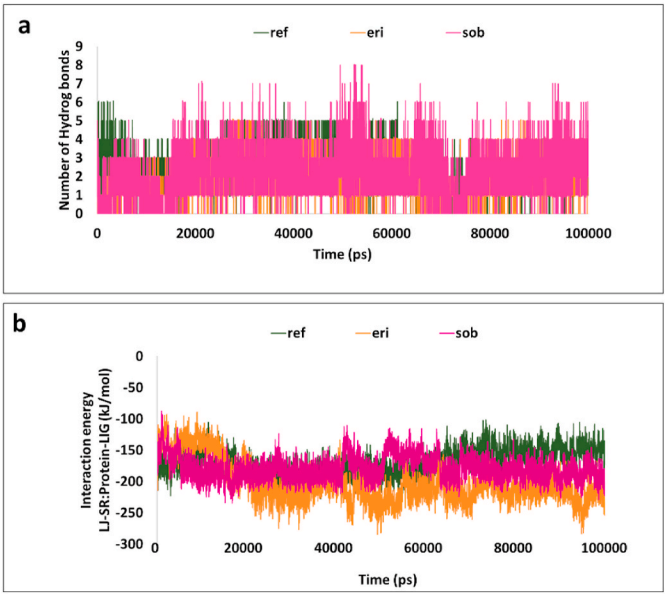

Fig. 3. MDS promoted hydrogen bond number and interaction energy calculations. (a) Profiles of the number of hydrogen bonds of the three system during the entire simulation. (b) Interaction energy between the protein and the ligand during the 100-ns simulation run.

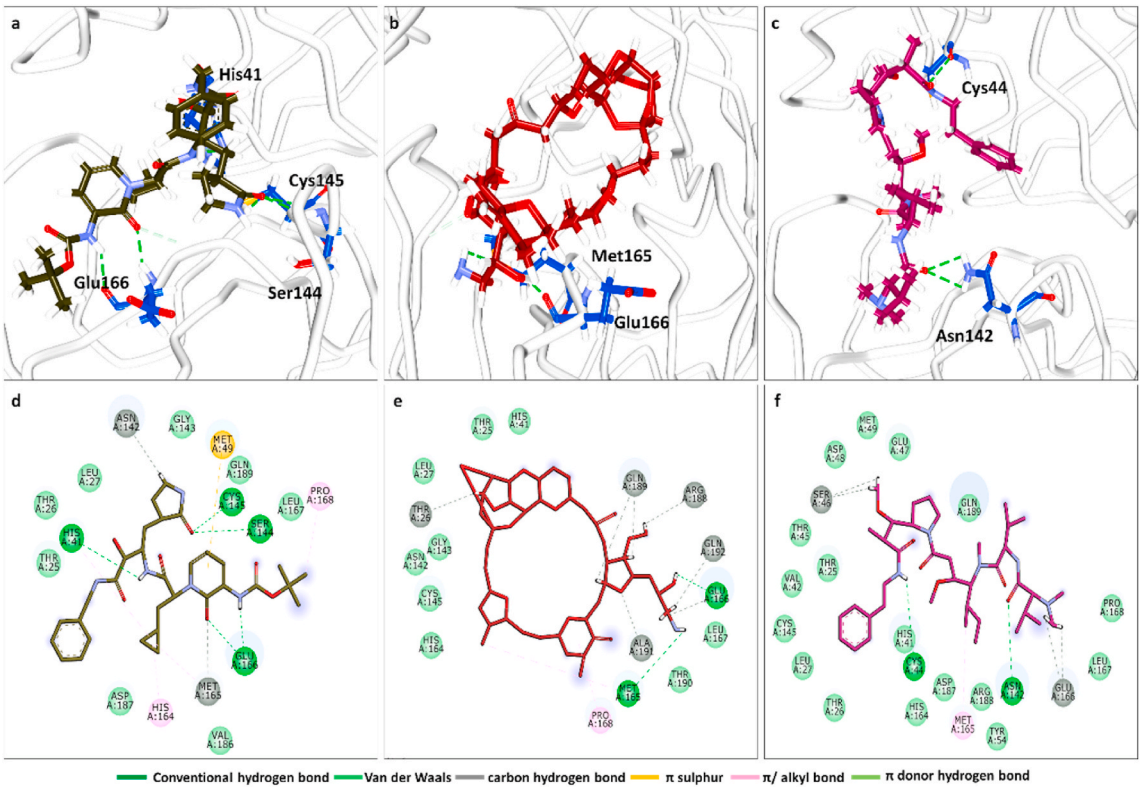

Fig. 4. Intermolecular interactions between the key residues of protein, PDB ID: 6Y2F, and the ligands. The intermolecular hydrogen bond interactions of ref, eri, and sob are shown in (a), (b), and (c), respectively. The comprehensive interactions of ref, eri, and sob are illustrated in (d), (e), and (f), respectively.

der Waals interactions and firmly nestled the ligand at the binding pocket, as shown in Fig. 4d.

Compound eri formed hydrogen bond interactions with Met165 and Glu166, respectively, established by an acceptable bond length, as shown in Fig. 4b and Table 2. The residue Pro168 formed a π-alkyl interaction with the ligand, helping to stabilise the position of the compound at the binding pocket. The residues Thr26, Arg188, Gly189, Ala191 and Gln192 formed carbon hydrogen bonds. Additionally, the residues Thr25, Leu27, His41, Asn142, Gly143, Cys145, His164, Leu167, and Thr190, assisted in the appropriate positioning of the ligand at the active site, as shown in Fig. 4e.

The compound sob generated hydrogen bond interactions with Cys44 and Asn142 with a permissible limit, as depicted in Fig. 4c and Table 2. The key residue, Met165, prompted an alkyl interaction with the ligand. The residues Ser46 and Glu166 generated carbon hydrogen bond. The residues such as Thr25, Thr26, Leu27, His41, Val42, Thr45, Glu47, Asp48, Met49, Cys145, Leu167, Pro168, His164, Arg188, Asp187, and Gln189 held the ligand via van der Waals interactions, positioning the ligand at the binding pocket of the target, as shown in Fig. 4f.

To gain additional insights into the binding of the putative inhibitors at the binding pocket of the protein, the distance between the hydrogen bond interacting atoms and the ligand atoms was measured. This analysis revealed that the initial distance was greater, varying between 0.2 and 0.8 nm, and a steady state was reached during the progression of the simulation run, as shown in Figs. 5 and 6. The eri structure generated hydrogen bond interactions with adjacent residues Met165 and Glu166, respectively. The distance between Met165 and its corresponding ligand atom was approximately 0.6 nm until 15,000 ps and dropped thereafter. Remarkably, from 20,000 ps, the bond distance was maintained at approximately 0.3 nm, with an average of 0.26 nm, as shown in Fig. 5a. Glu166 formed a relatively stable interaction with its ligand atom from 20,000 ps, with an average of 0.26 nm. Notably, the distance in the initial simulation run appeared to be longer and projected a length of

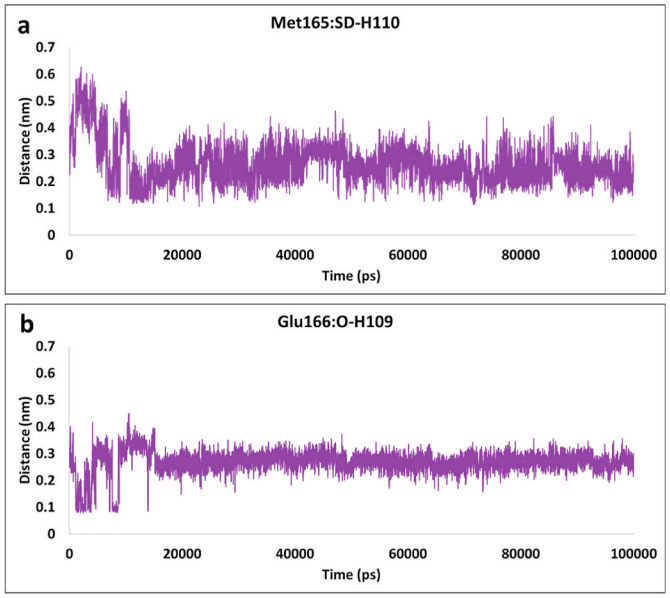

Fig. 5. MDS-derived hydrogen bond distance analysis of eri and the key residues at the binding pocket (a) Distance between Met165 and its corresponding ligand atom H110. (b) Distance between Glu166 and ligand atom H109.

0.4 nm, which then declined and reached a steady profile from 20,000 ps, as shown in Fig. 5b.

Likewise, the distance analysis of the interacting residues forming the hydrogen bond between the target protein and sob was reviewed. The modelling of residue Cys44 projected a firm interaction with an average of 0.20 nm. The initial distance was observed at 0.5 nm, which gradually dropped at approximately 6500 ps, with no fluctuations

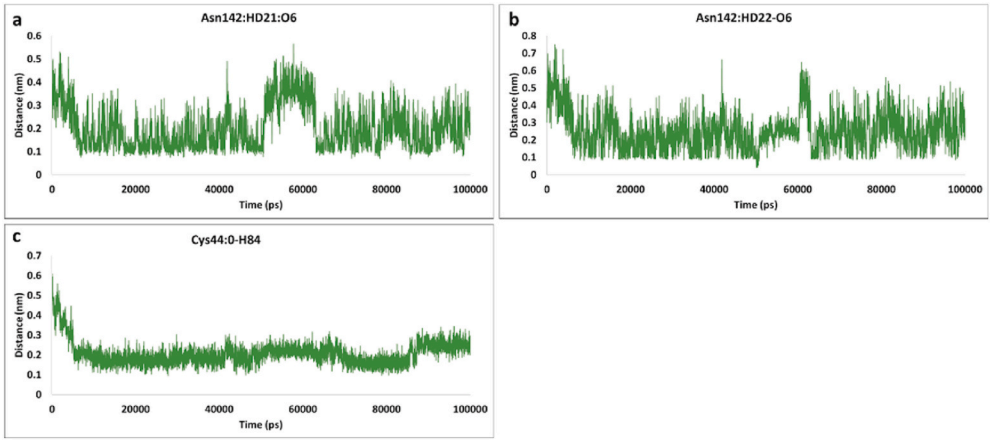

Fig. 6. MDS-derived hydrogen bond distance analysis between the sob and the key residues at the binding pocket (a) Distance between Asn142 and its corresponding ligand atom O6. (b) Distance between Ans142 and ligand atom O6. (c) Distance between Cys44 and ligand atom H84.

thereafter. The distance plot revealed an increase at approximately 87,120 ps, while it was within the acceptable limit of 0.3 nm, as shown in Fig. 6c. The residue Asn142 formed two hydrogen bond interactions with the same ligand atom O6. Asn142:HD21 demonstrated an average distance of 0.2 nm, with an increase between 45,000 ps and 60,000 ps, as shown in Fig. 6a. Similarly, the distance between Asn142:HD22 showed a steady profile with a marginal increase from 55,000 to 60,000 ps and projected an average of 0.25 nm, as shown in Fig. 6b. From these distance profiles, it can be stated that the key residues interact with the ligands by an acceptable length, indicating their strong interaction, as shown in Figs. 5 and 6.

3.9. Interaction energy analysis

Furthermore, to assess the strength of the interaction between the protein and the small molecule, the interaction energies were computed and read according to the term LJ-SR: protein-lig. All the systems displayed an interaction energy between −250 and −100 kJ/mol. The average value of the interaction energy for ref, eri, and sob was computed as −170, −203, and −179 kJ/mol, respectively, as illustrated in Fig. 3b. These findings suggest that the identified compounds have higher binding affinity toward the target than the co-crystallised compound, highlighting their usability as an alternative therapy for COVID-19.

3.10. Essential dynamics (EDs)

The function of a protein is governed by transformations between different conformations. The structure of a protein will show varying degrees of flexibility/rigidity, especially with respect to the residues at the binding pocket [47]. To understand the comprehensive motion of the protein utilised in the conformational space during the 100-ns

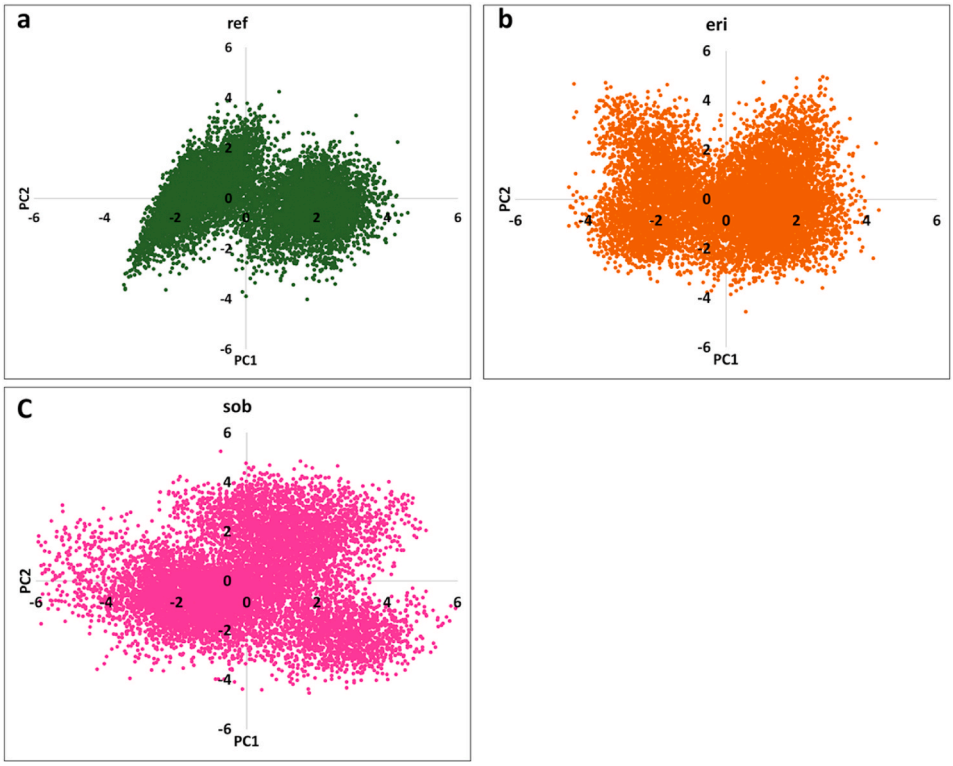

Fig. 7. Essential dynamic analysis. PC analysis of ref (a), eri (b), and sob (c).

simulation run, an ED analysis was performed using the two projection principal components (PCs), PC1 and PC2. PC1 and PC2 were computed by diagonalising the co-variance matrix of eigenvectors to specifically label the subspaces in which a major part of the protein dynamics occurs. The ED plots clearly indicated that the protein was localised in a minor conformational space. Nevertheless, the sob structure seems to have occupied relatively more conformational space along PC2, inferring that the protein might have moved across a wide range of conformational space before obtaining the equilibrated state [47], as shown in Fig. 7.

3.11. Free energy landscape

To gain further insight into the conformational transition behind the protein-ligand interaction, free energy landscape (FEL) descriptions are useful. FEL facilitates accurate details of the minimum energy conformations of biomolecular ensembles and are generated using the first two PCs, PC1 and PC2. In one study the Boltzmann inversion (F = -RT InP), where P is defined as the 2D probability distribution, pertaining to the first two PCs, PC1 and PC2, when taken as reaction coordinates [47]. Our findings demonstrate that the compounds, eri and sob, bind with the protein via a minimum free energy pathway, as shown in Fig. 8. The sob-protein complex occupied a wider conformational space along PC2. Notably, the energy minima are segregated through a smaller transition barrier, suggesting a smaller excursion. The FEL of the eri structure demonstrates a rigid bound complex when compared to a sob with a transition barrier. In brief, the FEL results elucidated the stable binding of the compounds at the protein binding site.

4. Discussion

Repurposing FDA drugs is an important strategy to discover effective drugs against SARS-CoV-2. Specifically, hindering the proteins involved in viral replication would be a valuable technique. Correspondingly, in the current work, we targeted the protein that is essential in the proteolytic process, the M^{pro} of SARS-CoV-2. Earlier, we have worked on M^{pro} and nsp16 (2′- O –methyltransferase) to discover potential inhibitors against SARS-CoV-2 [53–55].

Natural compounds offer a host of therapeutic applications, and many have been repurposed against COVID-19. Nevertheless, the potential of natural compounds extracted from marine habitats has not been well studied. Remarkably, even FDA approved marine drugs/derivatives and those in clinical trials offer to be a good alternative. Therefore, in the current study we utilised both approved marine drugs/derivatives and drugs in clinical trials to identify putative inhibitors that inhibit M^{pro}. Our thorough computational analysis yielded two compounds, sob and eri, as promising inhibitors against M^{pro}. It has been recently reported that eri is a potential inhibitor of M^{pro} [56].

Sob (auristatin PE or TZT-1027) is a synthetic product obtained from dolastatin 10, which acts as a vascular disrupting compound involved in the disintegration of vasculature within the tumour and demonstrates tubulin inhibitory potential [27,28]. Eri (E7389 or halichondrin B) is a natural polyether macrolide obtained from marine sponges. Preclinical animal model studies have demonstrated that eri has potent anticancer activity. It acts by irreversible antimitotic action, thereby causing cell death via the apoptotic pathway [27,28].

The binding pocket of SARS-CoV-2 M^{pro} comprises four subsites consisting of key residues [57–59]. Our identified inhibitors prompted crucial interactions with these residues through several interactions. Both compounds were accommodated in the binding site throughout the simulations, as shown in Fig. 9. The compound eri was held by the hydrogen bond interactions and alkyl and π alkyl interactions by the residues arising from the lower part of the active site, as shown in Fig. 10a, and is encircled by the residues via van der Waals interactions, facilitating strong positioning of the compound. Likewise, compound sob showed two hydrogen bond interactions with the residues from the top and bottom portions of the binding pocket, as shown in Fig. 10b. The residues from various other subsites prompted van der Waals interactions to firmly secure the compound at the binding pocket, as shown in Fig. 10b.

The compound eri generated interactions with the key residues Met165 and Glu166 rendered by hydrogen bonds, while the compound sob formed van der Waals interactions with Glu166 and alkyl interactions with Met165, respectively. Interactions with these residues have been reported to be beneficial for inhibiting M^{pro} [60–62]. Furthermore, Met165 additionally forms an alkyl interaction. The catalytic residues His41 and Cys145 demonstrated van der Waals interactions, favouring the inhibition of the viral target. Intriguingly, upon careful visual inspection of the interacting residues, it can be observed that compound eri has demonstrated hydrogen bond interactions and alkyl interactions with the residues emerging from domain II, while being clamped by van der Waals interactions with the residues from

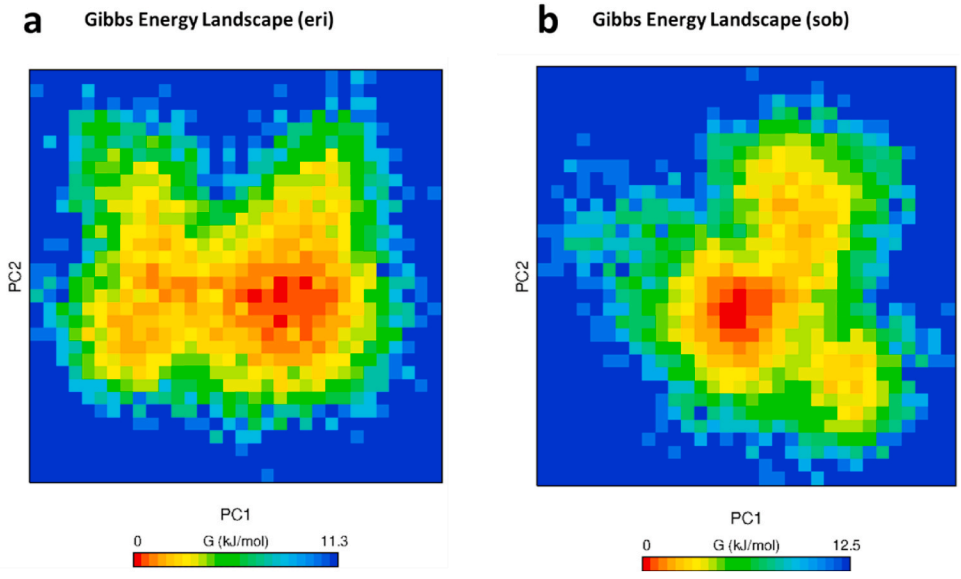

Fig. 8. Free energy landscapes of target protein bound to eri (a) and sob (b) during 100 ns MD simulation. Free energy is indicated in kJ/mol and represented by the colour code, from lower (red) to higher (blue) energy.

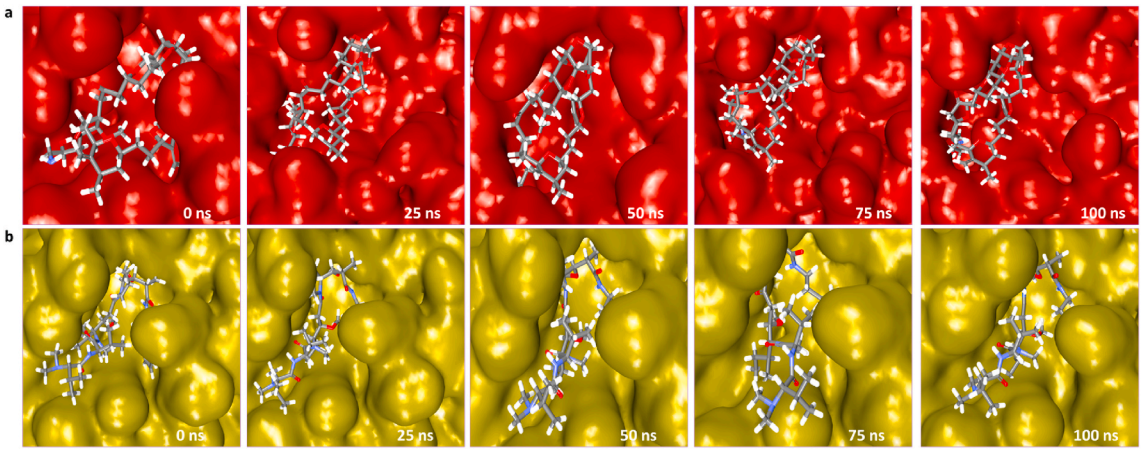

Fig. 9. Binding mode analysis of the small molecules, eri (a) and sob (b), at the binding pocket of the protein, PDB ID: 6Y2F.

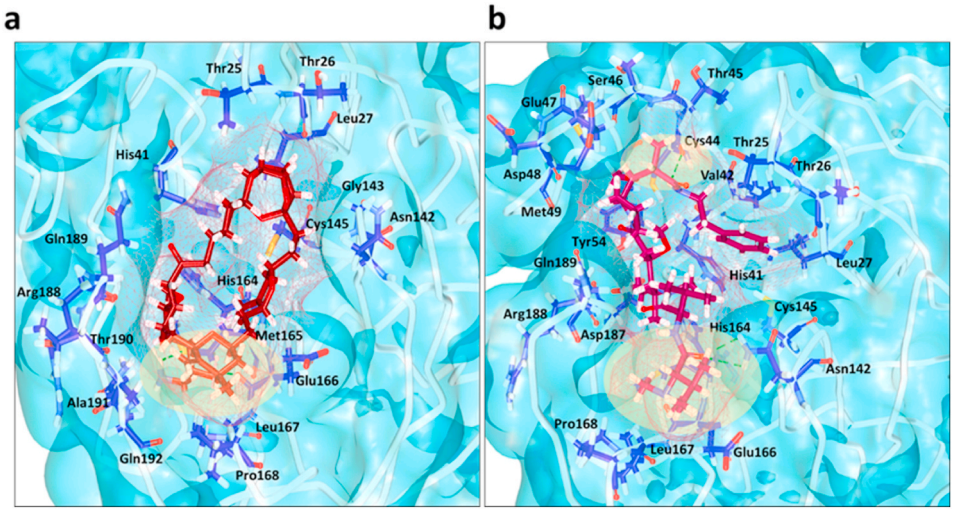

Fig. 10. Comprehensive intermolecular interactions between protein and ligand. (a) eri (b) sob. The surface of the protein, PDB ID: 6Y2F, is shown in light blue. The ligand surface is indicated in wire surface in light brown. The small molecules and the residues are shown as stick structures. The hydrogen bonds and the π/alkyl interactions are present in yellow.

other domains. Unlike eri, the sob forms hydrogen bond interactions with a pivotal residue from domain II, while it stretches to interact with Cys44 in domain I. Cys44 has been reported to be a conserved residue distributed within the M^{pro}s of SARS-CoV2/CoV, MERS-CoV, and SARS-like bat-CoV and exhibits a higher nucleophilic property than Cys145 [63]. Furthermore, the high reactivity of Cys44 and its vicinity to the substrate-binding pocket favours it as an attractive site for covalent linkage [63]. The two compounds are clamped by several other residues from different subsites, firmly holding the compounds at the binding pocket via hydrogen bonds. These findings provide substantial evidence for the use of marine derivatives to produce the desired inhibition.

Detailed MDS studies provide elegant evidence that the stability of the compounds is preserved during the simulations rendered by the RMSD and Rg profiles. The RMSF plots additionally support our findings by showing no wider variations.

Additionally, the FEL projected that the protein navigated through smaller conformational spaces prior to obtaining the ensemble-equilibrated state. Our results showed that the protein was in the energy-favoured conformations (red to orange spots) [64] with a few unfavourable conformations (dark blue spots), as shown in Fig. 8, [64]. Additionally, these compounds conferred a good docking score and binding energies as compared with the reference compound, elevating their SARS-CoV-2 therapeutic ability.

Furthermore, a detailed comparison was conducted to understand the structure–activity relationship **(**SAR) between the selected docked pose and the MDS-derived pose. Compound eri was generally static, whereas minor changes were noticed with respect to the groups from the free chain region, enabling a stable positioning at the binding pocket, as observed with the hydrogen bond residues (Fig. 11a and b). Furthermore, the Cys145 residue formed a π-alkyl interaction with the ligand but retained a van der Waals interaction in the MD pose. These findings shed light on the marginal movement of the ligand scaffold. Unlike eri, sob adopts a different conformation, prompting a carbon hydrogen bond interaction with Ser46 and producing hydrogen bond interactions with the key residue Asn142. The MD simulations also stabilised the ligand at the binding pocket firmly by adjusting the unfavourable acceptor-acceptor bond between the ligand and the residue Glu166 to van der Waals interactions. These dynamic movements have established a hydrogen bond interaction with residue Cys44. Interestingly, the residue Met165 retained its π-alkyl interaction in both the docked pose and the MD pose, indicating firm binding with the ligand (Fig. 11c and d).

The ADMET was analysed for the selected compounds along with the reference enabling the *ADMET Descriptors* module available on the DS, and the results are listed in Table 3. Furthermore, Lipinski's rule of five was calculated [65,66].

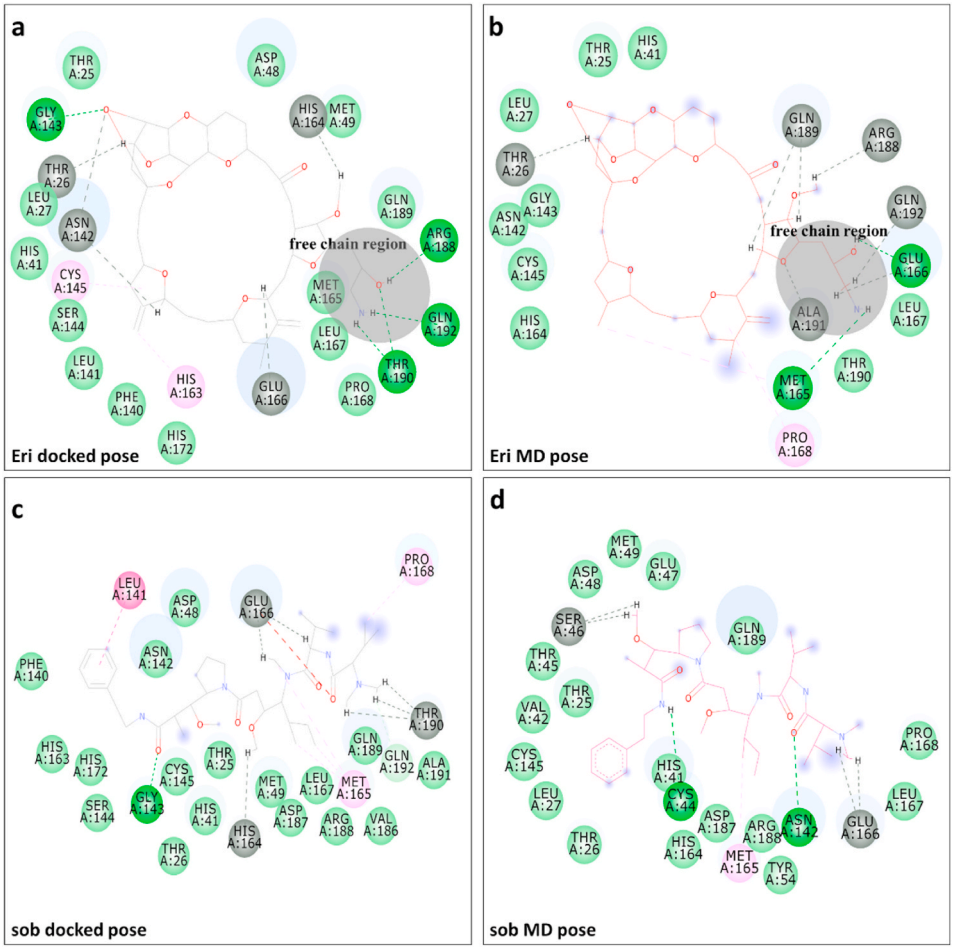

Fig. 11. Structure–activity relationship (SAR) comparing the docked pose (a and c) and the MD pose (b and d).

Table 3
Tabulation of ADMET and Lipinski rule of 5.

Compound	Solubility	BBB	CYP2D6	Hepatotoxicity	Absorption	PPB	Mol weight	HBD	HBA	LOGP	Molar Refractivity
Cocrystal	4	4	X	X	3	X	554	0	12	0.88	135.39
eri	2	4	X	X	2	X	729	0	12	3.27	171.25
sob	3	4	X	X	2	X	701	2	10	2.14	185.89

Upon performing the novelty search in PubChem Compounds [67] and ChemSpider [68] with SMILES of the compounds as input, it was clear that these compounds have not been reported as prospective drugs against SARS-CoV-2. Taken together, our findings are evidence of the suitability of marine products for further SARS-CoV-2 clinical studies. These compounds can be adapted as starting structures for the design and synthesis of new chemical scaffolds.

5. Conclusion

Diseases caused by zoonotic viruses, such as SARS-CoV-2, are a global menace [69,70]. The present study involves the use of marine drugs that are FDA approved and/ or are currently in clinical trials. Their efficacy was computationally evaluated against SARS-CoV-2 M^{pro} to identify potential compounds. Our detailed analysis revealed two compounds, eri and sob, as potential therapeutic compounds, and demonstrated good docking scores and displayed stable binding stabilities. The ED studies disclosed their compactness and relatively static conformation, which indicates their high potential as SARS-CoV-2 main protease inhibitors. Based on the results of our study, we propose two compounds, eri and sob, as potential leads. Further studies on these compounds, in particular experimental validation and optimisation, could be a promising strategy to fight COVID-19. Additionally, these compounds can act as chemical starting spaces for the design of new compounds.

Declaration of competing interest

The authors report no conflicts of interest in this work.

Acknowledgement

This research was supported by the Bio & Medical Technology Development Program of the National Research Foundation (NRF) & funded by the Korean government (MSIT) (No. NRF-2018M3A9A7057263).

This research was supported by the Neurological Disorder Research Program of the National Research Foundation (NRF) funded by the Korean Government (MSIT) (2020M3E5D9080660).

Appendix A. Supplementary data

Supplementary data to this article can be found online at https://doi.org/10.1016/j.compbiomed.2021.104525.

References

[1] A.E. Gorbalenya, S.C. Baker, R.S. Baric, R.J. de Groot, C. Drosten, A.A. Gulyaeva, B. L. Haagmans, C. Lauber, A.M. Leontovich, B.W. Neuman, D. Penzar, S. Perlman, L. L.M. Poon, D.V. Samborskiy, I.A. Sidorov, I. Sola, J. Ziebuhr, The species Severe acute respiratory syndrome-related coronavirus: classifying 2019-nCoV and naming it SARS-CoV-2, Nat. Microbiol 1 (2020) 536–544, https://doi.org/10.1038/s41564-020-0695-z.

[2] N. Chen, M. Zhou, X. Dong, J. Qu, F. Gong, Y. Han, Y. Qiu, J. Wang, Y. Liu, Y. Wei, J. Xia, T. Yu, X. Zhang, L. Zhang, Epidemiological and clinical characteristics of 99 cases of 2019 novel coronavirus pneumonia in Wuhan, China: a descriptive study, Lancet 395 (10223) (2020) 507–513, https://doi.org/10.1016/S0140-6736(20)30211-7.

[3] L. Wang, Y. Wang, D. Ye, Q. Liu, Review of the 2019 novel coronavirus (SARS-CoV-2) based on current evidence, Int. J. Antimicrob. Agents 55 (6) (2020), https://doi.org/10.1016/j.ijantimicag.2020.105948.

[4] J. Zheng, SARS-coV-2: an emerging coronavirus that causes a global threat, Int. J. Biol. Sci. 16 (10) (2020) 1678–1685, https://doi.org/10.7150/ijbs.45053.

[5] M. Pal, G. Berhanu, C. Desalegn, V. Kandi, Severe acute respiratory syndrome coronavirus-2 (SARS-CoV-2): an update, Cureus 12 (2020), https://doi.org/10.7759/cureus.7423 e7423–e7423.

[6] R.A. Khailany, M. Safdar, M. Ozaslan, Genomic Characterization of a Novel SARS-CoV-2. Gene Reports, 2020, https://doi.org/10.1016/j.genrep.2020.100682.

[7] E.J. Snijder, P.J. Bredenbeek, J.C. Dobbe, V. Thiel, J. Ziebuhr, L.L.M. Poon, Y. Guan, M. Rozanov, W.J.M. Spaan, A.E. Gorbalenya, Unique and conserved features of genome and proteome of SARS-coronavirus, an early split-off from the coronavirus group 2 lineage, J. Mol. Biol. 331 (5) (2003) 991–1004, https://doi.org/10.1016/S0022-2836(03)00865-9.

[8] F.K. Yoshimoto, The proteins of severe acute respiratory syndrome coronavirus-2 (SARS CoV-2 or n-COV19), the cause of COVID-19, Protein J. 39 (2020) 198–216, https://doi.org/10.1007/s10930-020-09901-4.

[9] I. Astuti, Ysrafil, Severe Acute Respiratory Syndrome Coronavirus 2 (SARS-CoV-2): an overview of viral structure and host response, Diabetes Metab. Syndr. 14 (2020) 407–412, https://doi.org/10.1016/j.dsx.2020.04.020.

[10] Y. Chen, Q. Liu, D. Guo, Emerging coronaviruses: genome structure, replication, and pathogenesis, J. Med. Virol. 92 (2020) 418–423, https://doi.org/10.1002/jmv.25681.

[11] Y.F. Tu, C.S. Chien, A.A. Yarmishyn, Y.Y. Lin, Y.H. Luo, Y.T. Lin, W.Y. Lai, D. M. Yang, S.J. Chou, Y.P. Yang, M.L. Wang, S.H. Chiou, A review of sars-cov-2 and the ongoing clinical trials, Int. J. Mol. Sci. 21 (7) (2020), https://doi.org/10.3390/ijms21072657.

[12] K.G. Arun, C.S. Sharanya, J. Abhithaj, D. Francis, C. Sadasivan, Drug repurposing against SARS-CoV-2 using E-pharmacophore based virtual screening, molecular docking and molecular dynamics with main protease as the target, J. Biomol. Struct. Dyn. (2020) 1–12, https://doi.org/10.1080/07391102.2020.1779819.

[13] Catherine Z. Chen, P. Shinn, Z. Itkin, R. Eastman, R. Bostwick, L. Rasmussen, R. Huang, M. Shen, X. Hu, K.M. Wilson, B. Brooks, H. Guo, T. Zhao, C. Klumpp-Thomas, A. Simeonov, S.G. Michael, D.C. Lo, M. Hall, W. Zheng, Drug Repurposing Screen for Compounds Inhibiting the Cytopathic Effect of SARS-CoV-2. bioRxiv, 2020.

[14] Catherine Z. Chen, M. Xu, M. Pradhan, K. Gorshkov, J.D. Petersen, M.R. Straus, W. Zhu, P. Shinn, H. Guo, M. Shen, C. Klumpp-Thomas, S.G. Michael, J. Zimmerberg, W. Zheng, G.R. Whittaker, Identifying SARS-CoV-2 entry inhibitors through drug repurposing screens of SARS-S and MERS-S pseudotyped particles, ACS Pharmacol. Transl. Sci. 3 (6) (2020) 1165–1175, https://doi.org/10.1021/acsptsci.0c00112.

[15] S. Dotolo, A. Marabotti, A. Facchiano, R. Tagliaferri, A Review on Drug Repurposing Applicable to COVID-19. Brief. Bioinform, 2020, https://doi.org/10.1093/bib/bbaa288.

[16] M. Kandeel, M. Al-Nazawi, Virtual screening and repurposing of FDA approved drugs against COVID-19 main protease, Life Sci. 251 (2020), https://doi.org/10.1016/j.lfs.2020.117627.

[17] Z. Li, X. Li, Y. Huang, Y. Wu, R. Liu, L. Zhou, Y. Lin, Identify Potent SARS-CoV-2 Main Protease Inhibitors via Accelerated Free Energy Perturbation-Based Virtual Screening of Existing Drugs, bioRxiv, 2020.

[18] S. Mohapatra, P. Nath, M. Chatterjee, N. Das, D. Kalita, P. Roy, S. Satapathi, Repurposing therapeutics for COVID-19: rapid prediction of commercially available drugs through machine learning and docking, PloS One 15 (11) (2020), https://doi.org/10.1101/2020.04.05.20054254.

[19] S. Rampogu, K.W. Lee, Old drugs for new purpose—fast pace therapeutic identification for SARS-CoV-2 infections by pharmacophore guided drug repositioning approach, Bull. Korean Chem. Soc. n/a 42 (2) (2021) 212–226, https://doi.org/10.1002/bkcs.12171.

[20] T.U. Singh, S. Parida, M.C. Lingaraju, M. Kesavan, D. Kumar, R.K. Singh, Drug repurposing approach to fight COVID-19, Pharmacol. Rep. 72 (2020) 1479–1508, https://doi.org/10.1007/s43440-020-00155-6.

[21] J. Sultana, S. Crisafulli, F. Gabbay, E. Lynn, S. Shakir, G. Trifirò, Challenges for drug repurposing in the COVID-19 pandemic era, Front. Pharmacol. 11 (2020), 588654, https://doi.org/10.3389/fphar.2020.588654.

[22] D. Bojkova, K. Klann, B. Koch, M. Widera, D. Krause, S. Ciesek, J. Cinatl, C. Münch, Proteomics of SARS-CoV-2-infected host cells reveals therapy targets, Nature 583 (2020) 469–472, https://doi.org/10.1038/s41586-020-2332-7.

[23] L. Zhang, D. Lin, X. Sun, U. Curth, C. Drosten, L. Sauerhering, S. Becker, K. Rox, R. Hilgenfeld, Crystal structure of SARS-CoV-2 main protease provides a basis for design of improved a-ketoamide inhibitors, Science 80 (2020), https://doi.org/10.1126/science.abb3405.

[24] Z. Jin, X. Du, Y. Xu, Y. Deng, M. Liu, Y. Zhao, B. Zhang, X. Li, L. Zhang, C. Peng, Y. Duan, J. Yu, L. Wang, K. Yang, F. Liu, R. Jiang, Xinglou Yang, T. You, Xiaoce Liu, Xiuna Yang, F. Bai, H. Liu, Xiang Liu, L.W. Guddat, W. Xu, G. Xiao, C. Qin, Z. Shi, H. Jiang, Z. Rao, H. Yang, Structure of Mpro from SARS-CoV-2 and discovery of its inhibitors, Nature 582 (2020) 289–293, https://doi.org/10.1038/s41586-020-2223-y.

[25] Z. Guo, The modification of natural products for medical use, Acta Pharm. Sin. B 7 (2) (2017) 119–136, https://doi.org/10.1016/j.apsb.2016.06.003.

[26] J.-Y. Lee, B. Orlikova, M. Diederich, Signal transducers and activators of transcription (STAT) regulatory networks in marine organisms: from physiological observations towards marine drug discovery, Mar. Drugs 13 (8) (2015), https://doi.org/10.3390/md13084967.

[27] A.M.S. Mayer, K.B. Glaser, C. Cuevas, R.S. Jacobs, W. Kem, R.D. Little, J. M. McIntosh, D.J. Newman, B.C. Potts, D.E. Shuster, The odyssey of marine pharmaceuticals: a current pipeline perspective, Trends Pharmacol. Sci. 31 (6) (2010) 255–265, https://doi.org/10.1016/j.tips.2010.02.005.

[28] H. Malve, Exploring the ocean for new drug developments: marine pharmacology, J. Pharm. BioAllied Sci. 8 (2) (2016) 83–91, https://doi.org/10.4103/0975-7406.171700.

[29] J. Yasuhara-Bell, Y. Lu, Marine compounds and their antiviral activities, Antivir. Res. 86 (3) (2010) 231–240, https://doi.org/10.1016/j.antiviral.2010.03.009.

[30] S.P. De Lira, M.H.R. Seleghim, D.E. Williams, F. Marion, P. Hamill, F. Jean, R. J. Andersen, E. Hajdu, R.G.S. Berlinck, A SARS-coronovirus 3CL protease inhibitor isolated from the marine sponge Axinella cf. corrugata: structure elucidation and synthesis, J. Braz. Chem. Soc. 18 (2) (2007), https://doi.org/10.1590/s0103-50532007000200030.

[31] J.Y. Park, J.H. Kim, J.M. Kwon, H.J. Kwon, H.J. Jeong, Y.M. Kim, D. Kim, W.S. Lee, Y.B. Ryu, Dieckol, a SARS-CoV 3CLpro inhibitor, isolated from the edible brown algae Ecklonia cava, Bioorg. Med. Chem. 21 (13) (2013) 3730–3737, https://doi.org/10.1016/j.bmc.2013.04.026.

[32] D. Gentile, V. Patamia, A. Scala, M.T. Sciortino, A. Piperno, A. Rescifina, Putative inhibitors of SARS-COV-2 main protease from a library of marine natural products: a virtual screening and molecular modeling study, Mar. Drugs 18 (4) (2020), https://doi.org/10.3390/md18040225.

[33] M.T. Khan, A. Ali, Q. Wang, M. Irfan, A. Khan, M.T. Zeb, Y.J. Zhang, S. Chinnasamy, D.Q. Wei, Marine natural compounds as potents inhibitors against the main protease of SARS-CoV-2—a molecular dynamic study, J. Biomol. Struct. Dyn. 39 (10) (2020) 3627–3637, https://doi.org/10.1080/07391102.2020.1769733.

[34] G. Muteeb, A. Alshoaibi, M. Aatif, M.T. Rehman, M.Z. Qayyum, Screening marine algae metabolites as high-affinity inhibitors of SARS-CoV-2 main protease (3CLpro): an in silico analysis to identify novel drug candidates to combat COVID-19 pandemic, Appl. Biol. Chem. (2020), https://doi.org/10.1186/s13765-020-00564-4.

[35] R. Vijayaraj, K. Altaff, A.S. Rosita, S. Ramadevi, J. Revathy, Bioactive compounds from marine resources against novel corona virus (2019-nCoV): in silico study for corona viral drug, Nat. Prod. Res. (2020), https://doi.org/10.1080/14786419.2020.1791115.

[36] S. Rampogu, S.M. Kim, M. Son, A. Baek, C. Park, G. Lee, Y. Kim, G.S. Kim, J.H. Kim, K.W. Lee, A computational approach with biological evaluation: combinatorial treatment of curcumin and exemestane synergistically regulates ddx3 expression in cancer cell lines, Biomolecules (2020), https://doi.org/10.3390/biom10060857.

[37] G. Wu, D.H. Robertson, C.L. Brooks, M. Vieth, Detailed analysis of grid-based molecular docking: a case study of CDOCKER - A CHARMm-based MD docking algorithm, J. Comput. Chem. (2003), https://doi.org/10.1002/jcc.10306.

[38] A. Puratchikody, D. Sriram, A. Umamaheswari, N. Irfan, 3-D structural interactions and quantitative structural toxicity studies of tyrosine derivatives intended for safe potent inflammation treatment, Chem. Cent. J. (2016), https://doi.org/10.1186/s13065-016-0169-9.

[39] D. Van Der Spoel, E. Lindahl, B. Hess, G. Groenhof, A.E. Mark, H.J.C. Berendsen, GROMACS: fast, flexible, and free, J. Comput. Chem. (2005), https://doi.org/10.1002/jcc.20291.

[40] S. Rampogu, S. Parameswaran, M.R. Lemuel, K.W. Lee, Exploring the therapeutic ability of fenugreek against type 2 diabetes and breast cancer employing molecular docking and molecular dynamics simulations. Evidence-based complement, Alternative Med. (2018), https://doi.org/10.1155/2018/1943203.

[41] S. Rampogu, K.W. Lee, Old drugs for new purpose—fast pace therapeutic identification for SARS-CoV -2 infections by pharmacophore guided drug repositioning approach, Bull. Kor. Chem. Soc. (2021), https://doi.org/10.1002/bkcs.12171.

[42] V. Zoete, M.A. Cuendet, A. Grosdidier, O. Michielin, SwissParam: a fast force field generation tool for small organic molecules, J. Comput. Chem. (2011), https://doi.org/10.1002/jcc.21816.

[43] M. Parrinello, Polymorphic transitions in single crystals: a new molecular dynamics method, J. Appl. Phys. 52 (1981) 7182, https://doi.org/10.1063/1.328693.

[44] B. Hess, H. Bekker, H.J.C. Berendsen, J.G.E.M. Fraaije, LINCS: a linear constraint solver for molecular simulations, J. Comput. Chem. 18 (1997) 1463–1472, https://doi.org/10.1002/(SICI)1096-987X(199709)18:12<1463::AID-JCC4>3.0.CO;2-H.

[45] W. Humphrey, A. Dalke, K. Schulten, VMD: visual molecular dynamics, J. Mol. Graph. (1996), https://doi.org/10.1016/0263-7855(96)00018-5.
[46] S. Rampogu, A. Baek, M. Son, C. Park, S. Yoon, S. Parate, K.W. Lee, Discovery of lonafarnib-like compounds: pharmacophore modeling and molecular dynamics studies, ACS Omega (2020), https://doi.org/10.1021/acsomega.9b02263.
[47] C.B. Mishra, P. Pandey, R.D. Sharma, M.Z. Malik, R.K. Mongre, A.M. Lynn, R. Prasad, R. Jeon, A. Prakash, Identifying the natural polyphenol catechin as a multi-targeted agent against SARS-CoV-2 for the plausible therapy of COVID-19: an integrated computational approach, Briefings Bioinf. (2020), https://doi.org/10.1093/bib/bbaa378.
[48] N.F. Dybdal-Hargreaves, A.L. Risinger, S.L. Mooberry, Eribulin mesylate: mechanism of action of a unique microtubule-targeting agent, Clin. Canc. Res. 21 (2015) 2445, https://doi.org/10.1158/1078-0432.CCR-14-3252. LP – 2452.
[49] J. Wu, X. Meng, R. Chu, S. Yu, Y. Wan, C. Song, G. Zhang, T. Zhao, Molecular dynamics simulation of the implantation of b-oriented ZSM-5 film modified α-quartz substrate surface with different modifiers, Front. Chem. (2019), https://doi.org/10.3389/fchem.2019.00746.
[50] I. Aier, P.K. Varadwaj, U. Raj, Structural insights into conformational stability of both wild-type and mutant EZH2 receptor, Sci. Rep. (2016), https://doi.org/10.1038/srep34984.
[51] M.Y. Lobanov, N.S. Bogatyreva, O.V. Galzitskaya, Radius of gyration as an indicator of protein structure compactness, Mol. Biol. (2008), https://doi.org/10.1134/S0026893308040195.
[52] Y.W. Dong, M.L. Liao, X.L. Meng, G.N. Somero, Structural flexibility and protein adaptation to temperature: molecular dynamics analysis of malate dehydrogenases of marine molluscs, Proc. Natl. Acad. Sci. U.S.A. (2018), https://doi.org/10.1073/pnas.1718910115.
[53] S. Rampogu, G. Lee, A.M. Kulkarni, D. Kim, S. Yoon, M.O. Kim, K.W. Lee, Computational approaches to discover novel natural compounds for SARS-CoV-2 therapeutics, ChemistryOpen 10 (2021) 593–599, https://doi.org/10.1002/open.202000332.
[54] S. Rampogu, K.W. Lee, Pharmacophore modelling-based drug repurposing approaches for SARS-CoV-2 therapeutics, Front. Chem. (2021).
[55] S. Rampogu, K.W. Lee, Old drugs for new purpose—fast pace therapeutic identification for SARS-CoV-2 infections by pharmacophore guided drug repositioning approach, Bull. Kor. Chem. Soc. (2021), https://doi.org/10.1002/bkcs.12171.
[56] P. Kalhotra, V.C.S.R. Chittepu, G. Osorio-Revilla, T. Gallardo-Velazquez, Field-template, QSAR, ensemble molecular docking, and 3D-RISM solvation studies expose potential of FDA-approved marine drugs as SARS-CoVID-2 main protease inhibitors, Molecules 26 (2021) 936, https://doi.org/10.3390/molecules26040936.
[57] A. Gimeno, J. Mestres-Truyol, M.J. Ojeda-Montes, G. Macip, B. Saldivar-Espinoza, A. Cereto-Massagué, G. Pujadas, S. Garcia-Vallvé, Prediction of novel inhibitors of the main protease (M-pro) of SARS-CoV-2 through consensus docking and drug reposition, Int. J. Mol. Sci. (2020), https://doi.org/10.3390/ijms21113793.
[58] A.M. Kanhed, D.V. Patel, D.M. Teli, N.R. Patel, M.T. Chhabria, M.R. Yadav, Identification of potential Mpro inhibitors for the treatment of COVID-19 by using systematic virtual screening approach, Mol. Divers. 1–19 (2020), https://doi.org/10.1007/s11030-020-10130-1.
[59] K. Świderek, V. Moliner, Revealing the molecular mechanisms of proteolysis of SARS-CoV-2 Mproby QM/MM computational methods, Chem. Sci. (2020), https://doi.org/10.1039/d0sc02823a.
[60] W. Rut, K. Groborz, L. Zhang, X. Sun, M. Zmudzinski, B. Pawlik, X. Wang, D. Jochmans, J. Neyts, W. Młynarski, R. Hilgenfeld, M. Drag, SARS-CoV-2 Mpro inhibitors and activity-based probes for patient-sample imaging, Nat. Chem. Biol. (2020), https://doi.org/10.1038/s41589-020-00689-z.
[61] M.D. Sacco, C. Ma, P. Lagarias, A. Gao, J.A. Townsend, X. Meng, P. Dube, X. Zhang, Y. Hu, N. Kitamura, B. Hurst, B. Tarbet, M.T. Marty, A. Kolocouris, Y. Xiang, Y. Chen, J. Wang, Structure and inhibition of the SARS-CoV-2 main protease reveal strategy for developing dual inhibitors against Mpro and cathepsin L, Sci. Adv. (2020), https://doi.org/10.1126/sciadv.abe0751.
[62] A.M. Sayed, H.A. Alhadrami, A.O. El-Gendy, Y.I. Shamikh, L. Belbahri, H. M. Hassan, U.R. Abdelmohsen, M.E. Rateb, Microbial natural products as potential inhibitors of SARS-CoV-2 main protease (Mpro), Microorganisms (2020), https://doi.org/10.3390/microorganisms8070970.
[63] N. Verma, J.A. Henderson, J. Shen, Proton-coupled conformational activation of SARS coronavirus main proteases and opportunity for designing small-molecule broad-spectrum targeted covalent inhibitors, J. Am. Chem. Soc. (2020), https://doi.org/10.1021/jacs.0c10770.
[64] A.M.H. Londhe, C.G. Gadhe, S.M. Lim, A.N. Pae, Investigation of molecular details of Keap1-Nrf2 inhibitors using molecular dynamics and umbrella sampling techniques, Molecules (2019), https://doi.org/10.3390/molecules24224085.
[65] B. Jayaram, T. Singh, G. Mukherjee, A. Mathur, S. Shekhar, V. Shekhar, Sanjeevini: a freely accessible web-server for target directed lead molecule discovery, BMC Bioinf. 13 (2012) S7, https://doi.org/10.1186/1471-2105-13-S17-S7.
[66] C.A. Lipinski, Lead- and drug-like compounds: the rule-of-five revolution, Drug Discov. Today Technol. (2004), https://doi.org/10.1016/j.ddtec.2004.11.007.
[67] S. Kim, P.A. Thiessen, E.E. Bolton, J. Chen, G. Fu, A. Gindulyte, L. Han, J. He, S. He, B.A. Shoemaker, J. Wang, B. Yu, J. Zhang, S.H. Bryant, PubChem substance and compound databases, Nucleic Acids Res. (2016), https://doi.org/10.1093/nar/gkv951.
[68] H.E. Pence, A. Williams, Chemspider: an online chemical information resource, J. Chem. Educ. (2010), https://doi.org/10.1021/ed100697w.
[69] D.S. Hui, E. I Azhar, T.A. Madani, F. Ntoumi, R. Kock, O. Dar, G. Ippolito, T. D. Mchugh, Z.A. Memish, C. Drosten, A. Zumla, E. Petersen, The continuing 2019-nCoV epidemic threat of novel coronaviruses to global health — the latest 2019 novel coronavirus outbreak in Wuhan, China, Int. J. Infect. Dis. (2020), https://doi.org/10.1016/j.ijid.2020.01.009.
[70] J.S. Mackenzie, D.W. Smith, COVID-19: a novel zoonotic disease caused by a coronavirus from China: what we know and what we don't, Microbiol. Aust (2020), https://doi.org/10.1071/MA20013. MA20013–MA20013.